*Semiconductor physics*

# Defect structure of high-resistance CdTe:Cl single crystals and $MoO_x$/CdTe:Cl/$MoO_x$ heterostructures according to the data of high-resolution X-ray diffractometry

**I.M. Fodchuk[1], A.R. Kuzmin[1], I.I. Hutsuliak[1], M.D. Borcha[1], V.O. Kotsyubynsky[2]**

*[1]Yuriy Fedkovych Chernivtsi National University,*
*2, Kotsiubynsky str., 58012 Chernivtsi, Ukraine*
*[2]Vasyl Stefanyk Precarpathian National University,*
*57, Shevchenko str., 76018 Ivano-Frankivsk, Ukraine*
*Corresponding author e-mail: ifodchuk@ukr.net*

**Abstract.** Clorine doped CdTe single crystals (CdTe:Cl) were grown by the traveling heater method. $MoO_x$/CdTe:Cl/$MoO_x$ films were deposited using the reactive magnetron sputtering technique. The defect structure of the obtained single crystals and heterostructures was investigated using high-resolution X-ray diffractometry. The optimized models of dislocation systems in the CdTe:Cl single crystals were constructed based on the Thompson tetrahedron. The distribution of the intensity of diffracted X-rays as a function of reciprocal space coordinates and rocking curves was analyzed using the kinematic theory of X-ray scattering in real crystals. The experimental and theoretically predicted values of the helical dislocation densities in the CdTe:Cl and $MoO_x$/CdTe:Cl crystals with perfect and mosaic structures were compared. Two-fold increase in the dislocation concentration in the $MoO_x$/CdTe:Cl heterostructures as a result of compression deformations of the CdTe:Cl crystal lattice was found. The ~0.1 μm thick transition deformed layer at the boundary between the $MoO_x$ film and CdTe:Cl single crystal significantly affects the electrical and spectroscopic properties of the obtained systems as the materials for γ-radiation detection.

**Keywords:** high-resolution X-ray diffractometry, CdTe:Cl single crystals, rocking curves, $MoO_x$/CdTe:Cl heterostructure, γ-radiation detectors.

https://doi.org/10.15407/spqeo26.04.415
PACS 07.77.Ka, 07.85.-m, 61.05.-a, 61.05.C-, 61.72.Lk, 61.72.Mm

Manuscript received 14.09.23; revised version received 23.10.23; accepted for publication 22.11.23; published online 05.12.23.

## 1. Introduction

Improvement of single crystal growth technology creates prospects for production of highly sensitive strain gauges for monitoring mechanical stresses and deformations in thin-walled structures [1], in particular in flexible shells and plates [2]. Cadmium telluride and compounds based on it are suitable for practical application in detectors for non-destructive inspection of cracks and internal micro-defects [3], optical sensors and filters [4], high-precision diagnostic and interventional radiology equipment [5], *etc.*

Moreover, cadmium telluride films are used in atomic energy and nuclear dosimetry as well as solar energy. In particular, research on CdTe thin-film photo-voltaic solar cells has become popular in recent years due to the innovations achieved in the CdTe technology [6]. CdTe solar panels are now on par in performance and cost with polycrystalline silicon panels [7].

As is generally known, the structure of real materials is always distorted and imperfect due to the presence of different point and/or line defects. X-rays are an excellent tool for investigation of the structural parameters. X-ray diagnostics serves to control the material quality, in particular to determine the structural parameters, composition and character of the defect distribution both in bulk crystals [8] and quasi-two-dimensional (multilayer) structures. In disordered solid solutions based on pure metals or complex compounds, precise X-ray studies combined with other theoretical and experimental techniques provide important insights into the anisotropy of the elastic properties and surface energy.

*© V. Lashkaryov Institute of Semiconductor Physics of the NAS of Ukraine, 2023*
*© Publisher PH "Akademperiodyka" of the NAS of Ukraine, 2023*

Cadmium telluride single crystals are actively used to manufacture X- and γ-radiation detectors due to their ability to operate at room temperatures, unlike silicon counterparts [9–13]. However, CdTe single crystals typically have a large number of defects (small-angle boundaries and high dislocation densities), which affect detector quality. Although the methods of growing highly perfect crystals are being continuously improved, influence of the defect structure on the electrical and spectroscopic properties of detectors is an ever-present problem. One of the main disadvantages of manufacturing high-efficiency X- and γ-radiation detectors based on CdTe:Cl is the reverse ohmic contact problem. There are no metals that form ohmic contacts with CdTe:Cl without additional surface treatment. Therefore, molybdenum oxide ($MoO_x$) is used as an interlayer material for formation of high-quality electrical contacts with CdTe:Cl due to its high work function (5.2…6.0 eV). Its additional advantages are transparency in the visible spectral range and relatively low specific electrical resistance. X-ray analysis remains the most informative method in the study of defects in crystals [29, 30]. High-resolution diffractometry makes it possible to evaluate the types and concentrations of defects, the integral and local deformations, the bending radius of atomic planes, the density of dislocations, as well as the symmetry of the fields of dislocation-created static distortions [14, 15].

This paper presents the results of the study of the defect structure of CdTe:Cl single crystals and CdTe/$MoO_x$ heterostructures using high-resolution X-ray diffractometry. The number of deformations in the transition layer between molybdenum oxide and CdTe.

## 2. Materials and methods

The objects of investigations were 5×5×1 mm CdTe:Cl (111) single crystals with the resistivity $\rho = (2…4)\cdot10^9$ Ohm·cm grown by the traveling heater method (Acrorad, Japan) at room temperature [16, 17] as well as CdTe/$MoO_x$ heterostructures obtained by reactive magnetron sputtering [18, 19].

$MoO_x$ films were deposited on heated polished single-crystalline CdTe:Cl substrates by sputtering of pure molybdenum (99.99% Mo) at a constant voltage. A LeyBold–Heraeus Vacuum System filled with an argon/oxygen mixture was used. The vacuum chamber was pre-pumped down to a residual pressure of $5\cdot10^{-5}$ mbar before the deposition. The argon ion sputtering technique was used for preparation of CdTe:Cl single crystal surfaces. The argon and oxygen pressures in the chamber during sputtering were 0.240 and 0.034 Pa, respectively. The magnetron power was 120 W. The deposition was carried out for 5 min. The substrate temperature was 573 K. The final thickness of the $MoO_x$ coating was 100 nm. XRD (HT-XRD) experiments were carried out using an X'Pert PRO (Panalytical, Philips) diffractometer with a CuK$\alpha_1$ radiation source.

## 3. Results and discussion

### 3.1. Defect structure of CdTe:Cl single crystals

Distributions of the X-ray intensity for symmetric and asymmetric reflections $Ih(\omega)$ and $Ih(Q_x, Q_z)$ from the CdTe:Cl single crystals were measured to analyze the crystal defect structure. A strong diffuse background in the dependence $Ih(Q_x, Q_z)$ and blurring of coherent scattering regions in the $Ih(\omega)$ distributions were observed (Fig. 1a). Structural perfection of the samples was evaluated using the $Ih(\omega)$ peak parameters (FWHM ($W$), maximum intensity ($Ih_{max}$), integral intensity (β) (Table 1), and peak shape in the coherent scattering region) as well as analyzing the diffuse component of the X-ray scattering intensity (Fig. 1a).

The correspondence between the experimental and theoretical values of FWHM of the $Ih(\omega)$ distributions was a criterion for assessing the degree of crystal perfection. Two samples, namely the most perfect one (labeled as "perfect") and the one with a mosaic structure (labeled as "mosaic") were selected for further investigation and comparative analysis. Cadmium telluride

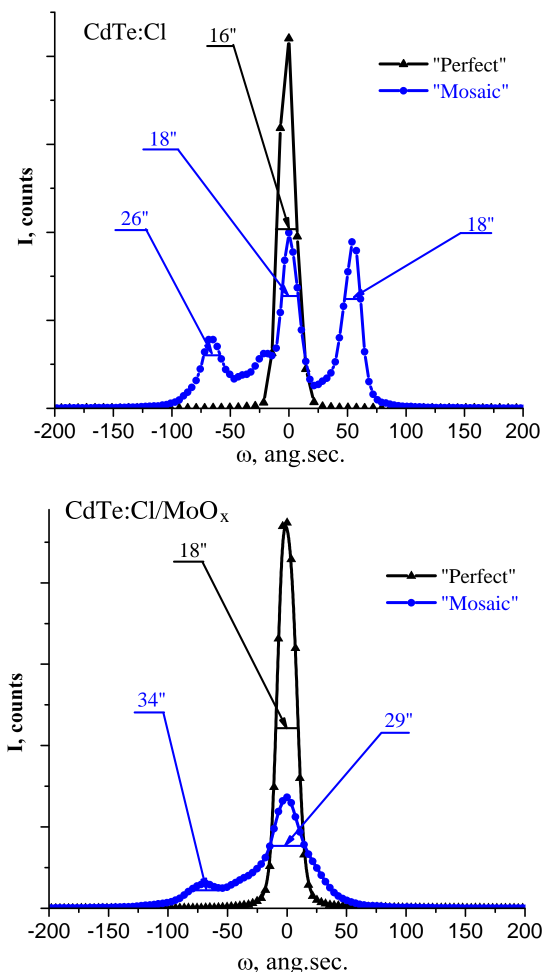


**Fig. 1.** XRD pattern of (a) "perfect" and "mosaic" CdTe:Cl single crystals; (b) CdTe:Cl/$MoO_x$ heterostructures based on the "perfect" and "mosaic" substrates ((333) reflection, CuK$\alpha_1$-radiation).

**Table 1.** Parameters of XRD patterns for CdTe:Cl single crystals and CdTe:Cl/$MoO_x$ heterostructures.

| Sample | Reflection | *W*, arc sec | β, arc sec |
|---|---|---|---|
| Before $MoO_x$ film deposition | | | |
| Perfect | 333 | 16 | 14.3 |
| | 331 | 17 | 17.5 |
| | 444 | 17 | 16.9 |
| Mosaic | 333 | 18 | 27.2 |
| | 331 | 24 | 45.2 |
| | 444 | 20 | 37.1 |
| After $MoO_x$ film deposition | | | |
| Perfect | 333 | 18 | 19.1 |
| | 331 | 19 | 21.4 |
| | 444 | 20 | 21.3 |
| Mosaic | 333 | 29 | 28.1 |
| | 331 | 32 | 36.1 |
| | 444 | 30 | 35.7 |

crystals usually contain various defects, inclusions of another phase, violations of stoichiometry *etc.* [20]. Presence of defects causes the asymmetry of the rocking curves and the appearance of oscillations of the scattered X-rays intensity ("tails"). Analysis of the diffuse scattering component allows estimating the defect sizes and concentrations [21]. Inclusions of another phase, packing defects, dislocations *etc.* can form in CdTe crystals during the growth process. However, dislocations make the most significant contribution to the change in the shape of the rocking curves as well as the appearance of a diffuse background around the coherent component in the central part of the map in Fig. 4.

Impact of the dislocation concentration on the increase of *W* and the change of $Ih(Q_x, Q_z)$ and $Ih(\omega)$ was analyzed using the theoretical approaches developed in [22, 23]. To determine the influence of dislocations on the formation of the X-ray intensity distribution, the dislocation line and Burgers vector $\vec{b}$ need to be parallel to the diffraction vector $\vec{g}$ as follows from the diffraction geometry (Fig. 2).

It was shown [24] that a dislocation system of perfect and partial dislocations in CdTe single crystals can be described using the Thompson tetrahedron. Fig. 2a shows all possible types of perfect and partial dislocations:

$$a/2[011] \rightarrow a/6[112] + a/6[\bar{1}2\bar{1}] \, , \quad (1)$$

$$a/2[011] + a/2[\bar{1}\bar{1}0] \rightarrow a/6[\bar{1}21] + a/6[\bar{1}\bar{2}1] + a/6[\bar{1}01] \, , \quad (2)$$

$$a/2[011] + a/2[011] \rightarrow a/6[121] + a/6[112] + a/3[001] \, . \quad (3)$$

Fig. 2b presents the unfolded Thompson tetrahedron and demonstrates more clearly the decomposition of a dislocation of the $a/2[011]$ type into Shockley partial dislocations $a/6[\bar{1}2\bar{1}]$ . In a symmetric geometry, the diffraction planes and the diffraction vector are parallel to the crystal surface. Therefore, two types of partial dislocations, namely screw Shockley and edge Frank dislocations (Fig. 2), have a dominant influence on the intensity distribution $Ih(Q_x, Q_z)$. In the asymmetric case, when the diffraction plane and vector are not parallel to the crystal surface, the contribution of perfect dislocations of the $a/2[011]$ type is added to $Ih(Q_x, Q_z)$.

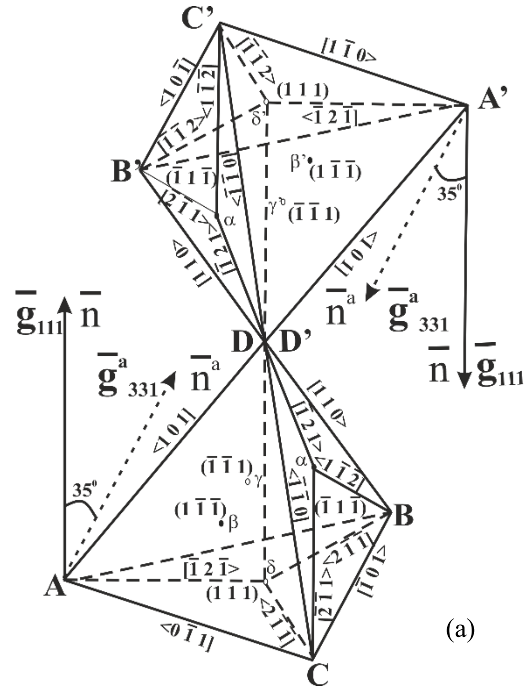


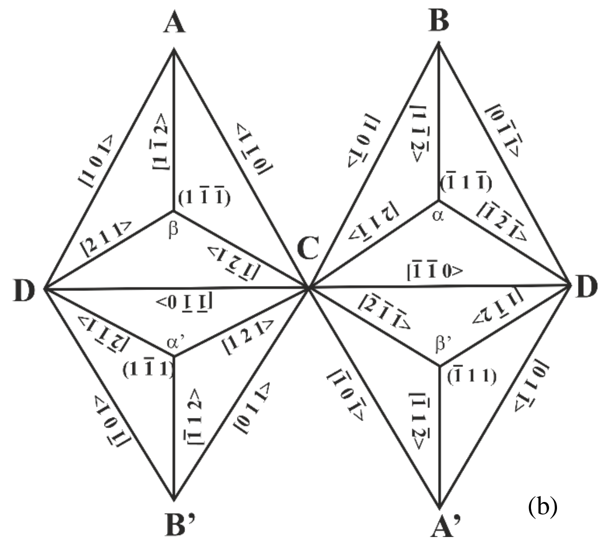


**Fig. 2.** Thompson tetrahedron and decomposition of perfect dislocations CD and DB into Shockley partial dislocations Dα and αC and a vertex dislocation βγ, and decomposition of CD into Frank partial dislocations Dδ and Shockley dislocations δC (a); scheme of position of two dislocation systems with the Burgers vectors and dislocation lines located in $(1\bar{1}\bar{1})$ and $(\bar{1}1\bar{1})$ planes (b).

The Thompson tetrahedron plot was used to construct models of a dislocation system that causes the formation of the observed X-ray scattered patterns at a certain crystallographic orientation [24]. Two optimal models with two systems of dislocations were selected: a) perfect 60-degree dislocations with the Burgers vectors $\bar{b}_1 = a/2[\bar{1}\,\bar{1}\,0]$ and $\bar{b}_2 = a/2[011]$, which lines are in $(1\,\bar{1}\,\bar{1})$ and $(\bar{1}\,1\,\bar{1})$ planes; b) partial Frank dislocations $\bar{b}_{\mathrm{F}} = a/3[111]$, which lines are oriented in $\langle 0\,\bar{1}\,1]$ and $[\bar{1}\,01\rangle$ directions. Such dislocations can also be located in the small-angle boundaries between blocks [24].

The experimental dependence $Ih(\omega)$ for the "mosaic" sample (Fig. 1) demonstrates a strong diffuse background of the intensity distribution in the region of coherent scattering. This indicates high densities of dislocations and their inhomogeneous spatial distribution. The X-ray intensity changes for the "mosaic" sample can also be caused by dislocations at the interblocks boundaries. The average density of the chaotically distributed dislocations is estimated as follows [25]:

$$N_G = \frac{W_G^2}{9|\vec{b}|^2}, \qquad (4)$$

where $\vec{b}$ is the Burgers vector of the dislocations.

In the case of "mosaic" crystal, the dislocation density $N_G$ was calculated for the most perfect block (Table 1).

The calculated values of $N_G$ for the "perfect" and "mosaic" CdTe:Cl single crystal samples are listed in Table 2. The densities $N_S$ of helical dislocations in these samples were calculated (Table 2) using the Williamson–Hall plot (Fig. 3) based on the value of inclination angle α of mosaic blocks [26]:

$$N_S = \frac{\alpha^2}{4.35|\vec{b}|^2}. \qquad (5)$$

**Table 2.** Calculated dislocation densities in CdTe:Cl single crystals and CdTe:Cl/$MoO_x$ heterostructures.

| Sample | Reflection | $N_G$, cm$^{-2}$, $10^5$ | $N_S$, cm$^{-2}$, $10^5$ |
|---|---|---|---|
| Before $MoO_x$ film deposition | | | |
| Perfect | 333 | 3.9 | 4.4 |
| | 331 | 5.3 | |
| | 444 | 4.1 | |
| Mosaic | 333 | 5.8 | 4.9 |
| | 331 | 6.5 | |
| | 444 | 6.2 | |
| After $MoO_x$ film deposition | | | |
| Perfect | 333 | 4.2 | 9.9 |
| | 331 | 5.1 | |
| | 444 | 4.6 | |
| Mosaic | 333 | 14.1 | 12.1 |
| | 331 | 15.7 | |
| | 444 | 14.2 | |

The X-ray intensity distributions $Ih(Q_x, Q_z)$ (Fig. 4) were simulated using the Kryvoglaz kinematic theory, which describes both coherent and diffuse scattering of X-rays in crystals with high concentrations of dislocations. Since the density of dislocations is significant (about $10^5 \ldots 10^6$ cm$^{-2}$), the intensity distribution $Ih(Q_x, Q_z)$ was calculated using the Monte Carlo method (Fig. 4) taking into account relaxation of surface strain [27, 28].

Comparing the $Ih(Q_x, Q_z)$ maps (Fig. 4) for symmetric and asymmetric reflexes (Table 1), a significant broadening of the coherent component (central part) and differences in the distributions of the diffuse components are observed for asymmetric (331) reflection. This confirms the dominant influence of Shockley and Frank partial dislocations as well as perfect dislocations on the X-ray intensity distribution in the case of asymmetric diffraction geometry (Fig. 4b). Blurring of the diffuse component indicates the presence of defects of another type, dislocation loops, clusters, *etc.*

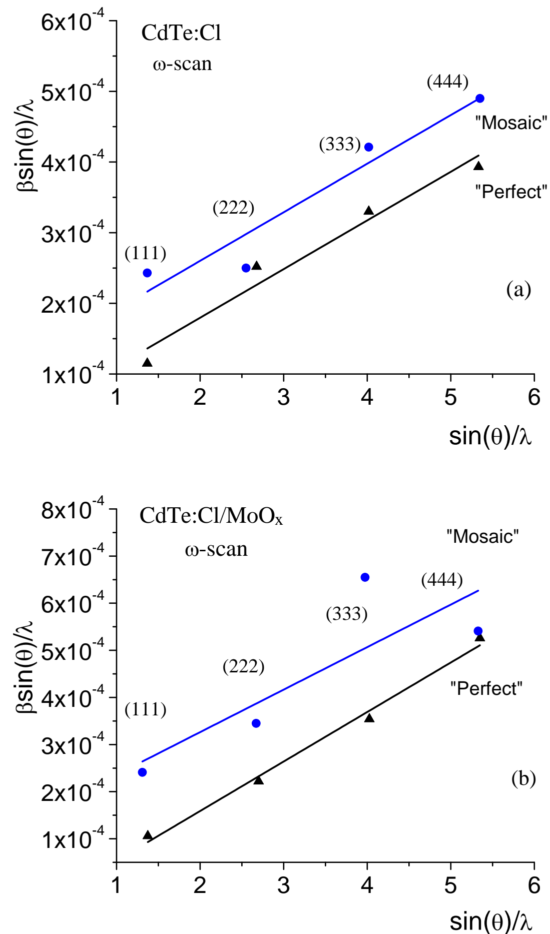


**Fig. 3.** Williamson–Hall plots for determination of helical dislocations density $N_S$ in (a) "perfect" and "mosaic" CdTe:Cl single crystal samples; and (b) CdTe:Cl/$MoO_x$ heterostructures based on the "perfect" and "mosaic" substrates (CuK$\alpha_1$-radiation).

(a) (b)

(c) (d)

**Fig. 4.** Experimental (a, c) and simulated (b, d) distributions $Ih(Q_x, Q_z)$ for "perfect" CdTe:Cl single crystal samples ((333) and (331) reflection, respectively). (Color online)

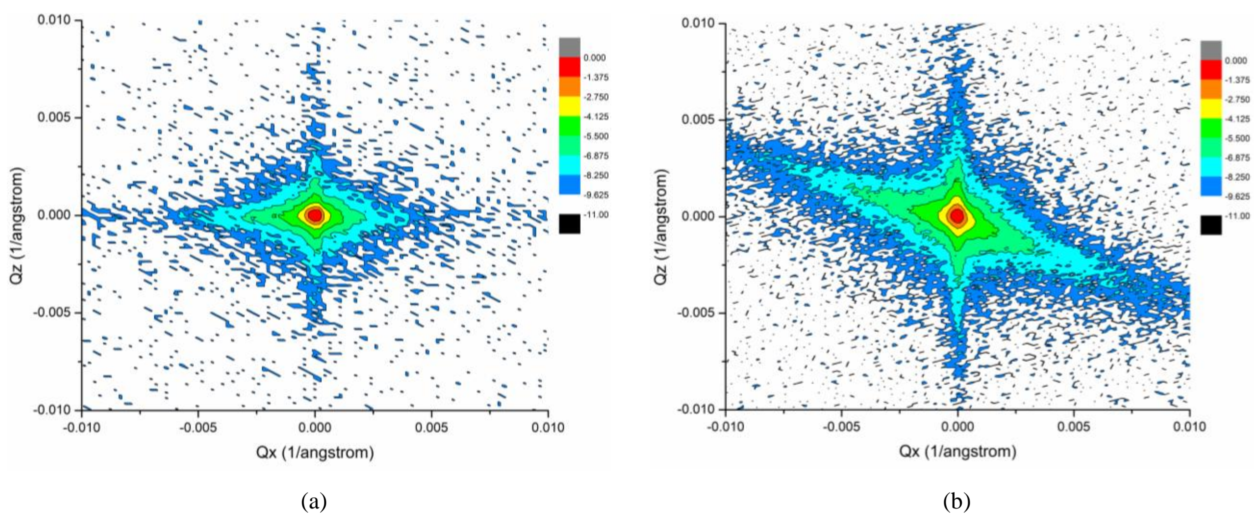


**Fig. 5.** Experimental distributions $Ih(Q_x, Q_z)$ for "perfect" CdTe:Cl/$MoO_x$ heterostructure after surface treatment. (a) and (b) correspond to the (333) and (331) reflections, respectively.(Color online)

### 3.2. Defect structure of CdTe:Cl/$MoO_x$ heterostructures

Deposition of $MoO_x$ layers on high-resistance CdTe:Cl single crystals is an important step in the development of X- and γ-radiation detectors. Therefore, it is important to analyze the defect structure of such heterostructures. Analysis of the diffuse scattering component (Fig. 1b) shows that ion etching carried out during sample preparation partly reduces stress in the surface layers.

The lattice parameter of $MoO_x$ ($a$ = 3.147 Å) is twice as small as the lattice parameter of CdTe ($a$ = 6.481 Å). Therefore, a significant compressive deformation of the crystal lattice occurs after deposition of molybdenum oxide on the CdTe surface transition layer. The observed increase in FWHM (Fig. 1b) is caused by appearance of various defects, in particular, misfit dislocations. The calculated values of the dislocation densities determined by the relation (4) and using the Williamson–Hall plot (Fig. 3b) are listed in Table 2. Deposition of $MoO_x$ films led to the increase of the densities of dislocations of both types. In particular, the density of dislocations in the CdTe:Cl/$MoO_x$ heterostructures based on the "perfect" CdTe:Cl single crystals increased twice, while three times increase was observed for the CdTe:Cl/$MoO_x$ based on the mosaic substrate. The intensity distribution $Ih(\omega)$ for the CdTe:Cl/$MoO_x$ based on the mosaic substrate (Fig. 1b) has a specific shape in the coherent scattering area and a strong diffuse background. This indicates significant violation of the structure in the near-surface layers of the heterostructures caused by inhomogeneously distributed dislocations (Table 2). The $Ih(Q_x, Q_z)$ distributions measured for symmetric and asymmetric reflections provide more complete information about the structural perfection of the studied samples (Fig. 5).

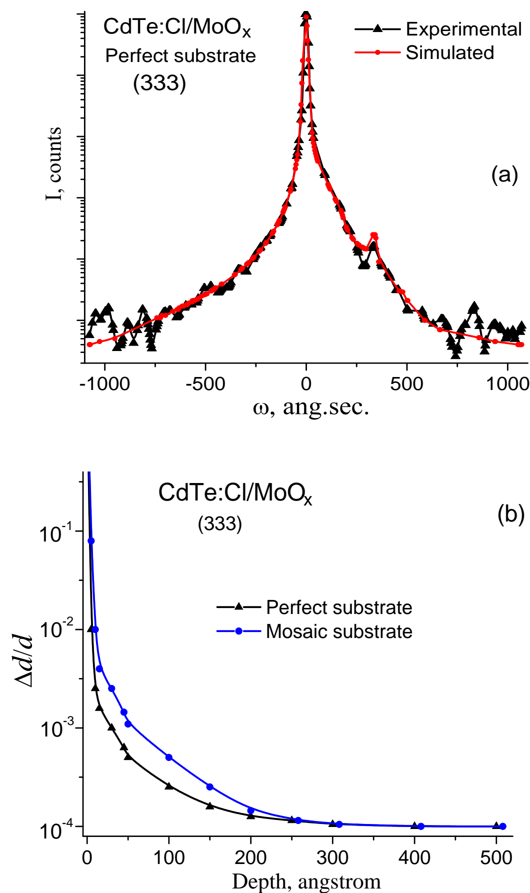


**Fig. 6.** Experimental and simulated rocking curves for CdTe:Cl/$MoO_x$ heterostructure based on the "perfect" substrate ((333) reflection) (a); deformation distributions in the near-surface layer of CdTe:Cl single crystal for "perfect" and "mosaic" based CdTe:Cl/$MoO_x$ heterostructures (b).

The experimental rocking curves of the CdTe:Cl/$MoO_x$ heterostructures were fitted using the semi-kinematic theory of X-ray scattering. The deformation distribution in the transition layer was calculated (Fig. 6a). The calculated deformation profile (the dependence of $\Delta d/d$ on the coordinate) in the oxide film/single crystal transition layer shows an exponential decline from $10^{-1}$ to $10^{-4}$ (Fig. 6b). This transition layer significantly affects the electrical and spectroscopic properties of the materials.

A promising way to minimize deformation is deposition of graphene layer on crystal surface before deposition of metal oxide film [29]. The defect structure of the substrates also affects the electrical and spectro-scopic characteristics of X- and γ-radiation detectors.

### 4. Conclusions

Models of dislocation systems in the CdTe:Cl single crystals were built based on the Thompson tetrahedron plot, which contains perfect 60-degree dislocations with the Burgers vectors $\bar{b}_1 = a/2[\bar{1}\,\bar{1}\,0]$ and $\bar{b}_2 = a/2[011]$, the lines in the $(1\,\bar{1}\,\bar{1})$ and $(\bar{1}\,1\,\bar{1})$ planes, as well as partial Frank dislocations with $\bar{b}_F = a/3[111]$ and the lines oriented in the $\langle 0\,\bar{1}\,1]$ and $[\bar{1}\,0\,1\rangle$ directions. The experimental distributions of scattered X-ray intensity ($Ih(\omega)$ and $Ih(Q_x, Q_z)$) were analyzed using the kinematic theory. The dislocation densities in the CdTe:Cl single crystals and CdTe:Cl/$MoO_x$ heterostructures of different perfection were estimated. The density of helical dislocations was $4.8\cdot10^5$ cm$^{-2}$ for the perfect CdTe:Cl single crystals and about $4.9\cdot10^5$ cm$^{-2}$ for the CdTe:Cl mosaic single crystals. Deposition of the $MoO_x$ films caused the increase in the dislocation density by more than two times. The density of helical dislocations was $9.9\cdot10^5$ cm$^{-2}$ for the CdTe:Cl/$MoO_x$ heterostructures based on a perfect crystal and $12.1\cdot10^5$ cm$^{-2}$ for the heterostructures based on a mosaic single crystal. The most probable reason for the formation of misfit deformations in the transition layers of the heterostructures are Shockley helical dislocations. The degree of structural perfection of the CdTe:Cl samples should be taken into account to obtain high-quality detectors of X- and γ-radiation.

**References**


1. Shats'kyi I.P., Shopa V.M., Velychkovych A.S. Development of full-strength elastic element section with open shell. *Strength Mater*. 2021. **53**. P. 277–282. https://doi.org/10.1007/s11223-021-00286-y.
2. Yang G., Park S.-J. Deformation of single crystals, polycrystalline materials, and thin films: A review. *Materials*. 2019. **12**. P. 2003. https://doi.org/10.3390/ma12122003.
3. Richtsmeier D., Guliyev E., Iniewski K., Bazalova-Carter M. Contaminant detection in non-destructive testing using a CZT photon-counting detector. *J. Instrum.* 2021. **16**. P. 01011. https://doi.org/10.1088/1748-0221/16/01/P01011.
4. Abbaspour S., Mahmoudian B., Islamian J.P. Cadmium telluride semiconductor detector for improved spatial and energy resolution radioisotopic imaging. *World J. Nucl. Med*. 2017. **16**. P. 101–107. https://doi.org/10.4103/1450-1147.203079.
5. Pelekhan B., Dutkiewicz M., Shatskyi I. *et al.* Analytical modeling of the interaction of a four implant-supported overdenture with bone tissue. *Mater.* 2022. **15**. P. 2398. https://doi.org/10.3390/ma15072398.
6. Mazur T., Mazur M., Halushchak M. Surface-barrier CdTe diodes for photovoltaics. *J. Nano-Electron. Phys*. 2023. **15**. P. 02006. https://doi.org/10.21272/jnep.15(2).02006.
7. Oklobia O., Kartopu G., Jones S. *et al*. Development of arsenic doped Cd(Se,Te) absorbers by MOCVD for thin film solar cells. *Sol. Energy Mater. Sol. Cells*. 2021. **231**. P. 111325. https://doi.org/10.1016/j.solmat.2021.111325.
8. Molodkin V.B., Olikhovskii S.I., Dmitriev S.V. *et al*. Dynamical effects in the integrated X-ray scattering intensity from imperfect crystals in Bragg diffraction geometry. I. Semi-dynamical model. *Acta Crystallogr. A: Found. Adv*. 2020. **76**(Pt 1). P. 45–54. https://doi.org/10.1107/S2053273319014281.
9. Gnatyuk V., Maslyanchuk O., Kulyk O. *et al*. Characterization of CdTe-based *p-n* junction-diode X/γ-ray detectors formed by frontside laser irradiation. *Proc. SPIE*. 2022. **12241**. P. 122410M. https://doi.org/10.1117/12.2633410.
10. Gnatyuk V., Maslyanchuk O., Solovan M., Brus V., Aoki T. CdTe x/γ-ray detectors with different contact materials. *Sensors*. 2021. **21**. P. 3518. https://doi.org/10.3390/s21103518.
11. Maslyanchuk O., Solovan M., Brus V. *et al*. Charge transport features of CdTe-based X- and γ-ray detectors with Ti and $TiO_x$ Schottky contacts. *Nucl. Instrum. Methods Phys. Res. A*. 2021. **988**. P. 164920. https://doi.org/10.1016/j.nima.2020.164920.
12. Gnatyuk V., Levytskyi S., Maslyanchuk O. *et al*. Performance of CdTe-based *p-n* junction-diode X/γ-ray detectors. *Proc. SPIE*. 2021. **12126**. P. 1212614. https://doi.org/10.1117/12.2615569.
13. Maslyanchuk O., Fodchuk I., Solovan M. *et al*. defects and charge collection in CdTe-based X- and gamma-ray detectors. *Proc. SPIE*. 2021. **12126**. P. 121260K. https://doi.org/10.1117/12.2615504.
14. Holý V. X-ray reflection curves of crystals with randomly distributed microdefects in the Bragg case. *Acta Cryst. A*. 1983. **39**. P. 642–646. https://doi.org/10.1107/S0108767383001312.
15. Borcha M.D., Solodkyi M.S., Balovsyak S.V. *et al*. Features of structural changes in mosaic Ge:Sb according to x-ray diffractometry and electron backscatter diffraction data. *SPQEO*. 2019. **22**. P. 381–386. https://doi.org/10.15407/spqeo22.04.381.
16. Gnatyuk D., Poperenko L., Yurgelevych I., Aoki T. Characterization of the surfaces of CdTe(111) single crystals after laser processing. *Proc. SPIE*. 2011. **8142**. P. 81421N. https://doi.org/10.1117/12.898417.
17. Shiraki H., Funaki M., Ando Y. *et al*. Improvement of the productivity in the THM growth of CdTe single crystal as nuclear radiation detector. *IEEE Trans. Nucl. Sci*. 2010. **57**. P. 395–399. https://doi.org/10.1109/TNS.2009.2035316.
18. Solovan M.M., Mostovyi A.I., Parkhomenko H.P. *et al*. Electrical and photoelectric properties of heterojunctions $MoO_x$/*n*-$Cd_{1-x}Zn_xTe$. *East Eur. J. Phys*. 2021. **1**. P. 34–42. https://doi.org/10.26565/2312-4334-2021-1-05.
19. Maslyanchuk O.L., Solovan M.M., Maistruk E.V. *et al*. Prospects of In/CdTe X- and γ-ray detectors with MoO Ohmic contacts. *Proc. SPIE*. 2018. **10612**. P. 106120V. https://doi.org/10.1117/12.2305085.
20. Kuciauskas D., Krasikov D. Spectroscopic and microscopic defect and carrier-lifetime analysis in cadmium telluride. *IEEE J. Photovolt*. 2018. **8**. P. 1754–1760. https://doi.org/10.1109/JPHOTOV.2018.2866180.
21. Booker I., Khoshroo L.R., Woitok J.F. *et al*. Dislocation density assessment via X-ray GaN rocking curve scans. *phys. status solidi (c)*. 2010. **7**. P. 1787–1789. https://doi.org/10.1002/pssc.200983615.
22. Fodchuk I., Kuzmin A., Hutsuliak I. *et al*. Defect structure of high-resistivity CdTe:Cl crystals according to the data of high-resolution X-ray diffractometry. *Proc. SPIE*. 2020. **11369**. P. 113691H. https://doi.org/10.1117/12.2553970.
23. Fodchuk I.M., Kuzmin A.R., Maslyanchuk O.L. *et al*. Influence of dislocation structure on electrical and spectroscopic properties of $MoO_X$/*p*-CdTe/$MoO_X$ heterostructures. *Phys. Chem. Solid State*. 2022. **23**. P. 144–149. https://doi.org/10.15330/PCSS.23.1.144-149.
24. Paulauskas T., Buurma C., Colegrove E. *et al*. Atomic scale study of polar Lomer–Cottrell and Hirth lock dislocation cores in CdTe. *Acta Cryst. A*. 2014. **70**. P. 524–531. https://doi.org/10.1107/S2053273314019639.
25. Šik O., Škvarenina L., Caha O. *et al*. Determining the sub-surface damage of CdTe single crystals after lap-ping. *J. Mater. Sci.: Mater. Electron*. 2018. **29**. P. 9652–9662. https://doi.org/10.1007/s10854-018-9002-7.
26. Takaki S., Masumura T., Tsuchiyama T. Dislocation characterization by the direct-fitting/modified

Williamson–Hall (DF/mWH) method in cold worked ferritic steel. *ISIJ Int.* 2019. **59**. P. 567–572. https://doi.org/10.2355/isijinternational.ISIJINT-2018-623.
27. Holy V., Pietsch U., Baumbach T. High-resolution X-ray scattering from thin films and multilayers. Springer: Berlin, 1999.
28. Holy V., Zhong Z., Bauer G., Ambacher O. High-resolution diffuse x-ray scattering from threading dislocations in heteroepitaxial layers. *Appl. Phys. Lett*. 2004. **85**(15). P. 3065–3067. https://doi.org/10.1063/1.1806279.
29. Brus V.V., Maslyanchuk O.L., Solovan M.M. *et al*. Graphene/semi-insulating single crystal CdTe Schottky-type heterojunction X- and γ-ray radiation detectors. *Sci. Rep*. 2019. **9**. P. 1065. https://doi.org/10.1038/s41598-018-37637-w.

**Authors and CV**

**Ihor M. Fodchuk**, Doctor of Sciences (Physics and Mathematics), Professor at the Department of Information Technologies and Computer Physics, Dean of the Faculty of Architecture, Construction, and Decorative and Applied Arts of the Yuriy Fedkovych Chernivtsi National University. Author of more than 150 publications. His research interests include theoretical and experimental studies of X-ray scattering by complex crystalline compounds and development of theoretical foundations of multilevel processing of experimental X-ray and electronic signals.
http://orcid/0000-0001-6772-6920

**Andrii R. Kuzmin**, Assistant at the Department of Information Technologies and Computer Physics of the Yuriy Fedkovych Chernivtsi National University. Author of 12 publications. His research interests include high-resolution X-ray diffractometry, defect structure of high-resistance CdTe single crystals, and ionizing radiation detectors.
E-mail: kuzay77736@gmail.com,
http://orcid.org/0000-0003-3146-0782

**Ivan I. Hutsuliak**, Candidate of Physical and Mathematical Sciences, Associate Professor at the Department of Information Technologies and Computer Physics of the Yuriy Fedkovych Chernivtsi National University. Author of more than 18 publications. His research interests include high-resolution X-ray diffractometry of structural features of single crystals and heterostructures.
E-mail: i.hutsuliak@chnu.edu.ua,
http://orcid/0000-0002-8156-9527

**Mariana D. Borcha**, Doctor of Sciences (Physics and Mathematics), Head of the Department of Information Technologies and Computer Physics of the Yuriy Fedkovych Chernivtsi National University. Author of more than 30 publications. Her research interests include multi-wavelength X-ray diffraction in deformed crystals and $A^2B^6$ and $A^3B^5$ compounds, study of the influence of deformation fields on multi-wavelength X-ray effects, extreme cases and the phase problem of multi-wavelength X-ray diffraction, diffraction of reflected electrons (Kikuchi diffraction), digital image processing, 3D visualization of experimental data, and computer tomography. E-mail: m.borcha@chnu.edu.ua,
http://orcid.org/0000-0001-6758-3173

**Volodymyr O. Kotsyubynsky**, Doctor of Sciences (Physics and Mathematics), Head of the Department of Materials Science and New Technologies, Professor of the Vasyl Stefanyk Precarpathian National University. Author of more than 120 publications. His research interests include measurement methodology and data interpretation of X-ray structural analysis, Mössbauer and X-ray fluorescence spectroscopy, low-temperature adsorption porometry, and impedance spectroscopy.
E-mail: volodymyr.kotsuybynsky@pnu.edu.ua,
http://orcid.org/0000-0001-6461-937X

**Authors' contributions**

**Fodchuk I.M.:** methodology, software, formal analysis, resources, writing-original draft preparation, visualization, writing-review and editing, supervision, project administration.
**Kuzmin A.R.:** methodology, software, validation, formal analysis, resources, writing-original draft preparation, visualization, writing-review and editing, supervision.
**Hutsuliak I.I.:** methodology, validation, formal analysis, investigation, resources, writing-review and editing.
**Borcha M.D.:** software, formal analysis, investigation, visualization, writing-original draft preparation.
**Kotsyubynsky V.O.:** methodology, validation, investigation, data curation, writing-original draft preparation, visualization, writing-review and editing, supervision.
All authors discussed the results and commented on the manuscript.

**Дефектна структура високоомних монокристалів CdTe:Cl та гетероструктур $MoO_x$/CdTe:Cl/$MoO_x$ за даними високороздільної X-променевої дифрактометрії**

**І.М. Фодчук, А.Р. Кузьмін, І.І. Гуцуляк, М.Д. Борча, В.О. Коцюбинський**

**Анотація.** Леговані хлором монокристали CdTe (CdTe:Cl) були вирощені методом рухомого нагрівача, а плівки $MoO_x$/CdTe:Cl/$MoO_x$ були нанесені за допомогою техніки реактивного магнетронного розпилення. Дефектну структуру отриманих монокристалів і гетероструктур досліджено методом високороздільної X-променевої дифрактометрії. Побудовано оптимізовані моделі дислокаційних систем на основі тетраедра Томпсона для монокристалів CdTe:Cl. Аналіз розподілу інтенсивності дифрагованого X-випромінювання як функції зворотних просторових координат і кривих гойдання проведено з використанням кінематичної теорії розсіяння X-випромінювання в реальних кристалах. Проведено порівняльний аналіз експериментальних та теоретично розрахованих значень густини гвинтових дислокацій для кристалів CdTe:Cl та $MoO_x$/CdTe:Cl з ідеальною та мозаїчною структурами. Для гетероструктур $MoO_x$/CdTe:Cl внаслідок компресійних деформацій кристалічної решітки CdTe:Cl виявлено збільшення концентрації дислокацій у 2 рази. Перехідний деформований шар на межі між плівкою $MoO_x$ і монокристалом CdTe:Cl товщиною близько 0,1 мкм істотно впливає на електричні та спектроскопічні властивості отриманих систем як матеріалів для реєстрації γ-випромінювання.

**Ключові слова:** високороздільна X-променева дифрактометрія, монокристали CdTe:Cl, криві гойдання, гетероструктури $MoO_x$/CdTe:Cl, детектори γ-випромінювання.